ELSEVIER

Journal of Quantitative Spectroscopy & Radiative Transfer 92 (2005) 293–310

Journal of Quantitative Spectroscopy & Radiative Transfer

www.elsevier.com/locate/jqsrt

Direct measurement of the Rayleigh scattering cross section in various gases

Maarten Sneep, Wim Ubachs*

Department of Physics and Astronomy, Laser Centre, Vrije Universiteit, De Boelelaan 1081, 1081 HV Amsterdam, The Netherlands

Received 2 April 2004; accepted 30 July 2004

Abstract

Using the laser-based technique of cavity ring-down spectroscopy extinction measurements have been performed in various gases straightforwardly resulting in cross sections for Rayleigh scattering. For Ar and N_2 measurements are performed in the range 470–490 nm, while for CO_2 cross sections are determined in the wider range 470–570 nm. In addition to these gases also for N_2O, CH_4, CO, and SF_6 the scattering cross section is determined at 532 nm, a wavelength of importance for LIDAR applications and combustion laser diagnostics. In O_2 the cross section at 532 nm is found to depend on pressure due to collision-induced light absorption. The obtained cross sections validate the cross sections for Rayleigh scattering as derived from refractive indices and depolarization ratios through Rayleigh's theory at the few %-level, although somewhat larger discrepancies are found for CO, N_2O and CH_4.

PACS: 94.10.Gb; 42.68.Mj; 33.20.Kf

Keywords: Rayleigh scattering; Cavity ring-down spectroscopy; Atmospheric molecules

*Corresponding author. Tel./fax: +31-20-444-7950.
E-mail addresses: sneep@nat.vu.nl (M. Sneep), wimu@nat.vu.nl (W. Ubachs).

0022-4073/$ - see front matter © 2004 Elsevier Ltd. All rights reserved.
doi:10.1016/j.jqsrt.2004.07.025

1. Introduction

The physical phenomenon of light scattering by particles of size small compared to the wavelength of the incident light, known as Rayleigh scattering, is well understood, both from a theoretical as well as an experimental perspective [1–3]. Although quantum mechanical expressions for the scattering cross sections related to corresponding oscillator strengths have been derived [4], the original derivation in terms of classical electromagnetic fields by Rayleigh still gives a proper quantitative expression for the cross section [1]. Fluctuations, or inhomogeneities, in the dielectric constant of a gas are held responsible for the scattering of light. The effects of density, temperature, molecular (re)-orientation, and the role of kinetics, causing elastic and inelastic scattering have primarily an effect on the spectral distribution of the scattered light. These phenomena give rise to splitting into several scattering components with Raman, Brillouin and Rayleigh-wing contributions, besides the central component, usually referred to as the Cabannes peak [5].

The original Rayleigh expression [1] for the total scattering cross section comprising all elastic and inelastic contributions directly relates to the index of refraction and through this relationship all phenomena of Rayleigh scattering have hitherto been analyzed quantitatively. Single or multiple scattering in the atmospheres of the Earth and planets [2,6], as well as laser-induced Rayleigh scattering for diagnosing complex flow fields, combustion processes and LIDAR applications [7] all rely on values for the refractive indices. Experimental values for Rayleigh scattering cross sections are extensively tabulated in the literature, in particular for a standardized form of air [8,9]. Two corrections are required to the original expression of Rayleigh. First there is the local field effect, in the theory of electromagnetism known as the Clausius–Mossotti, or the Lorentz–Lorenz correction [10], but for low-density gases this is a negligible effect. A second correction, related to the non-sphericity of molecules and its effect of depolarization were first studied by Strutt (Rayleigh's son) [11,12]. The accompanying increase in the cross section was analyzed by King [13], and is since known as the King correction factor.

Over the years refractive indices have been measured using interferometric techniques, and for many gases dispersion formulas have been composed. The resulting refractive indices, used to derive Rayleigh scattering cross sections, are at an accuracy considered sufficient for atmospheric radiative transfer calculations. Information on the correction factor for non-spherical molecules is sparse, however, and the dispersion of this factor is often ignored. For this reason experimental verification of the Rayleigh extinction by other means is warranted and this is one of the purposes of the present study. Direct determination of the scattering cross section is difficult, in view of the required calibration of quantum efficiencies of detectors and integration over a scattering volume. Recently it was demonstrated that values for Rayleigh scattering cross sections can directly be obtained from extinction measurements using the sensitive technique of cavity ring-down (CRD) absorption spectroscopy [14].

In the present work the same CRD-method is used to measure the Rayleigh scattering cross section in various gases. These measurements are an extension of the measurements performed earlier between 15 500 and 18 000 cm^{-1} in Ar, N_2 and SF_6 [14]. Here, the frequency range between 20 400 and 21 400 cm^{-1} for N_2 and Ar is added, to further test the predicted wavelength dependence—$\sigma \propto 1/\lambda^4$—of the Rayleigh scattering cross section. The scattering cross section of CO_2 is measured over a larger frequency range (17 500–18 200 and 20 400–21 400 cm^{-1}). This gas

is interesting from an astrophysical point of view, as the atmospheres of Mars and Venus consist mainly of CO_2. Also the correction factor for the non-sphericity is particularly large for CO_2. Finally, measurements of the scattering cross at 532 nm—the second harmonic of a Nd:YAG laser, a wavelength frequently used in LIDAR applications—in CO_2, N_2, Ar, N_2O, CH_4, CO, SF_6 and O_2 are performed as well.

2. The Rayleigh scattering cross section for atomic and molecular gases

In the late nineteenth century Rayleigh derived a cross section for particles of size small compared to the wavelength and in the electric dipole approximation [1]:

$$\sigma = \frac{32\pi^3}{3\lambda^4 N^2}(n-1)^2. \tag{1}$$

With N in molecule m^{-3} and λ in m, this gives the scattering cross section in m^2/molecule. In atmospheric physics, and in modern notation, the cross section is commonly expressed in cm^2 per molecule. With $\bar{\nu}$ in cm^{-1} and N in molecule cm^{-3}, the cross section becomes:

$$\sigma_{\bar{\nu}} = \frac{24\pi^3\bar{\nu}^4}{N^2}\left(\frac{n_{\bar{\nu}}^2-1}{n_{\bar{\nu}}^2+2}\right)^2 F_k(\bar{\nu}), \tag{2}$$

where also the local field correction and the King correction factor for the depolarization [7,13] is included.

The effects of local fields can be written in terms of the Lorentz–Lorenz relation for the classical molecular polarizability [10]:

$$\alpha_{SI} = \frac{3\varepsilon_0}{N}\left(\frac{n^2-1}{n^2+2}\right). \tag{3}$$

In most gases $n \approx 1$, and the error made by the approximation is small. For example in air the effect is at the level of 0.05% [9]. Note that α is the polarizability *per particle*, and that it is independent of the density. The refractive index n in (Eq. 3) is the refractive index at density N. The subscript SI indicates that this quantity is in SI units: $[\alpha_{SI}] = F\,m^2$. In literature, the volume polarizability is often used: $\alpha_{vol} \equiv \alpha_{SI}/4\pi\varepsilon_0$, which has the dimensions of a volume [15]. At first glance it would seem that the cross section depends on the density of the gas. However, it should be considered that the refractive index is a collective effect and that the Lorentz–Lorenz relation (3) gives the molecular polarizability for a *single* molecule and therefore (Eq. 2) is independent of the density. This equation can also be written in terms of the molecular volume polarizability:

$$\sigma_{\bar{\nu}} = \frac{128}{3}\pi^5\alpha_{vol}^2\bar{\nu}^4 \tag{4}$$

with α_{vol} in cm^3 and $\bar{\nu}$ in cm^{-1}, explicitly showing that the scattering cross section is independent of the density.

The issue of non-spherical particles can also be addressed in terms of the molecular polarizability, which is then written as a 3×3 tensor α_{ij}, which carries a diagonal component α_{ii}, a symmetric component $\alpha_{ij}^{(s)} = \alpha_{ji}^{(s)}$ and an anti-symmetric component $\alpha_{ij}^{(a)} = -\alpha_{ji}^{(a)}$. The anisotropy of

the polarizability affects the scattering cross section and the distribution of the scattered light. The effect is commonly expressed in terms of the depolarization ratio $\rho = I_\perp/I_\parallel$, the incomplete polarization of light scattered by molecules at 90 °, as studied by Strutt [11,12]. The depolarization ratios can be expressed in terms of elements of the polarizability tensor along the principal axes of the molecule, α_{ii} [2,7,13]:

$$\rho_n = \frac{2\sum_i \alpha_{ii}^2 - 2\sum_{i<j}\alpha_{ii}\alpha_{jj}}{4\sum_i \alpha_{ii}^2 + \sum_{i<j}\alpha_{ii}\alpha_{jj}}, \qquad \rho_p = \frac{\sum_i \alpha_{ii}^2 - \sum_{i<j}\alpha_{ii}\alpha_{jj}}{3\sum_i \alpha_{ii}^2 + 2\sum_{i<j}\alpha_{ii}\alpha_{jj}}. \tag{5}$$

It is then easily verified that the depolarization for natural light ρ_n relates to that of polarized light ρ_p via: $\rho_n = 2\rho_p/(1+\rho_p)$ and $\rho_p = \rho_n/(2-\rho_n)$. The depolarization ratios depend on the frequency of the primary light, just as the refractive index depends on frequency, but the functional form may be very different. The refractive index and the polarizability are again related by (Eq. 3), but now for non-spherical particles, and α has to be replaced by $\bar{\alpha} = \frac{1}{3}\sum_i \alpha_{ii}$ [16].

For linear and symmetric top molecules, a simplification can be made. With $\alpha_\parallel = \alpha_{11}$ the polarizability along the symmetry axis of the molecule, $\alpha_\perp = \alpha_{22} = \alpha_{33}$ the polarizability perpendicular to it, and $\gamma = \alpha_\parallel - \alpha_\perp$, one finds:

$$\rho_p = \frac{\gamma_{\bar{\nu}}^2}{15\bar{\alpha}_{\bar{\nu}}^2 + \frac{4}{3}\gamma_{\bar{\nu}}^2}. \tag{6}$$

Integration of the full intensity distribution leads to the scattering cross section including the King correction factor, which is expressed as

$$F_k(\bar{\nu}) = \frac{6+3\rho_n(\bar{\nu})}{6-7\rho_n(\bar{\nu})} = \frac{3+6\rho_p(\bar{\nu})}{3-4\rho_p(\bar{\nu})} = 1 + 2\left(\frac{\gamma_{\bar{\nu}}}{3\bar{\alpha}_{\bar{\nu}}}\right)^2. \tag{7}$$

Both expressions for the depolarization for natural- and polarised light, ρ_n and ρ_p, can be used in the formula for the King factor, producing the same correction to the scattering cross section, as is to be expected from symmetry arguments: the total scattering cross section cannot depend on the state of polarization of the incident light. Note that $F_k \geqslant 1$, implying that the scattering cross section will always be larger for non-spherical particles compared to spherical particles with the same refractive index. With the theoretical result of (Eq. 2), one can calculate the extinction coefficient in a gas, if the refractive index at a specified density, the density and the depolarization ratio are known. For nitrogen ρ_n at a wavelength of 500 nm is equal to 0.0213, leading to a King correction factor of 1.035 [8].

In the above-cited derivations the motion nor internal quantized excitation of the molecules is considered. A more sophisticated description of light scattering [3] reveals that the spectrum is centered around the frequency of the driving light, but molecular motion adds other spectral features. A central unshifted peak, usually referred to as the *Cabannes* peak, is accompanied by side features, originating from scattering off adiabatic density fluctuations, or acoustic waves. The exact shift, depolarization, intensity and line shape of these inelastic Brillouin peaks depend on scattering angle, adiabatic index $\tilde{\gamma} = c_p/c_v$ and pressure. For 1 bar nitrogen at 273 K illuminated by 500 nm light, the maximum shift with respect to the incident radiation is found to be 0.04 cm^{-1} [17]. Additional spectral components at larger separation are the features of Raman scattering. Two different types of Raman scattering exist: the vibrational Raman peak has a separation of

2330.7 cm^{-1} from the central structure in N_2, while the separation of the rotational Raman structure is much smaller, at about 8 cm^{-1} in N_2 [18], and a red-shifted *Stokes* and a blue-shifted *anti-Stokes* component occur. The cross section for Raman scattering is relatively small. For example in N_2 the ratio is 2.3% for rotational- and 0.07 % for vibrational Raman scattering, both for incident radiation of 500 nm [19]. Weak overtone vibrational Raman lines ($\Delta v = 2$) have been observed as well [20], but these spectral components are even much weaker than the main branches with $\Delta v = 1$.

All of these light scattering phenomena, further including Rayleigh-wing scattering and Placzek trace scattering, have specific differential cross sections and depolarization ratios, that all relate to components of the polarizability tensor α_{ij}. Polarization features of all distinct phenomena were recently reviewed and tabulated by Miles et al. [7]. Elements of the polarizability tensor can be calculated from the quantum mechanical structure of the atom or molecule. The transition strengths of all possible optical transitions have to be included in the calculation, including those to the continuum states [21,16]. From the polarizability tensor, the refractive index can be calculated by means of the Lorentz–Lorenz relation (3). Also the depolarization ratio and Raman scattering cross section can be calculated from the tensor [22,19]. Hence, quantum chemical computations can be used to calculate these properties from first principles, a procedure which has been pursued for hydrogen and nitrogen [23–26]. In Ref. [26] a Rayleigh scattering cross section in nitrogen is calculated, using only ab initio procedures, yielding 6.2×10^{-27} cm^2 $molecule^{-1}$, again at 500 nm. This value is 10% lower than the experimental value.

In the present study a measurement is performed on the total extinction cross section of gaseous species. The extinction relates to the sum of all scattering modes discussed above—Cabannes, Brillouin, Raman and Rayleigh-wing scattering—and absorption. It is assumed that no absorptions occur in the wavelength regions investigated in this work; for the closed shell gaseous species investigated here the first electronically excited states are above the region probed by visible light. On the other hand, in the visible range only extremely weak overtone vibrational transitions can be probed, much weaker in cross section than Rayleigh scattering. Hence, the measured extinction can be considered equal to the total Rayleigh scattering; this is the basic assumption underlying the present work. As will be shown in oxygen collision-induced phenomena add to the total extinction cross section. For the analysis of atmospheric measurements, the Rayleigh scattering cross section is usually calculated from the refractive index, using Eqs. (2) and (7), with an appropriate King correction. Refractive indices are commonly measured by interferometric techniques, such as described in Ref. [27], while the depolarization ratio is measured directly through the ratio of the perpendicular and parallel polarizations of the scattered radiation at 90° as described in references [16,21]. In the following, we will refer to values for the cross section thus derived as *n*-based Rayleigh cross sections. Our method, discussed in the next section, measures the extinction directly, and provides an independent verification of the Rayleigh scattering cross section.

3. The experimental method

The experiment was conducted with a generic pulsed cavity-ring down (CRD) experiment, similar to the setup previously used in Ref. [14]. For the general methods of cavity ring-down

spectroscopy we refer to a recent review [28]. In CRD spectroscopy a light pulse from a pulsed laser is coupled into a stable resonator and subsequently an optical decay transient is produced, exiting at the rear end of the optical cavity. This decay transient typically has the form of an exponential, with a rate of decay depending on the mirror reflectivity $\mathscr{R}_{\bar{\nu}}$ and the length of the cavity d. In case of an absorbing medium with cross section $\sigma_{\bar{\nu}}$ and density N filling the entire void between the mirrors the loss rate of the resonator equals:

$$\beta_{\bar{\nu}} = c|\ln \mathscr{R}_{\bar{\nu}}|/d + c\sigma_{\bar{\nu}}N. \tag{8}$$

This result is only valid if the observed decay transient has indeed the functional form of a single exponential decay. For this purpose the alignment of the resonator was optimized toward mono-exponential decay with the aid of on-line monitoring during alignment as described by Naus et al. [29].

To separate the contribution of Rayleigh extinction from the decay rate of the empty cell (the first term in Eq. (8), related to the non-perfect mirror reflectivity $\mathscr{R}_{\bar{\nu}}$), the decay rate is constantly monitored during a pressure ramp. While the cell is filled with gas over a period of about 15 min, the losses due to scattering by the gas increase linearly with the density, while the losses on the mirrors remain constant. Note that the pressure ramp itself does not have to be linear in time, although best results are achieved with a smooth ramp. During the pressure ramp the frequency of the laser is kept at a fixed position and between 1000 and 1200 measurements of the loss rate—with a pulsed laser at a 10 Hz repetition frequency—are performed. Three typical pressure ramps are shown in Fig. 1.

A Nd:YAG pumped pulsed dye laser (Quanta-Ray system) with a bandwidth of 0.05 cm^{-1} and a pulse duration of 5 ns was used to excite the ring down cavity. A grating spectrometer in Echelle configuration with a neon spectral reference lamp was employed for frequency calibration. For the measurements at 18 788.4 cm^{-1} (corresponding to 532.2 nm), the second harmonic of the

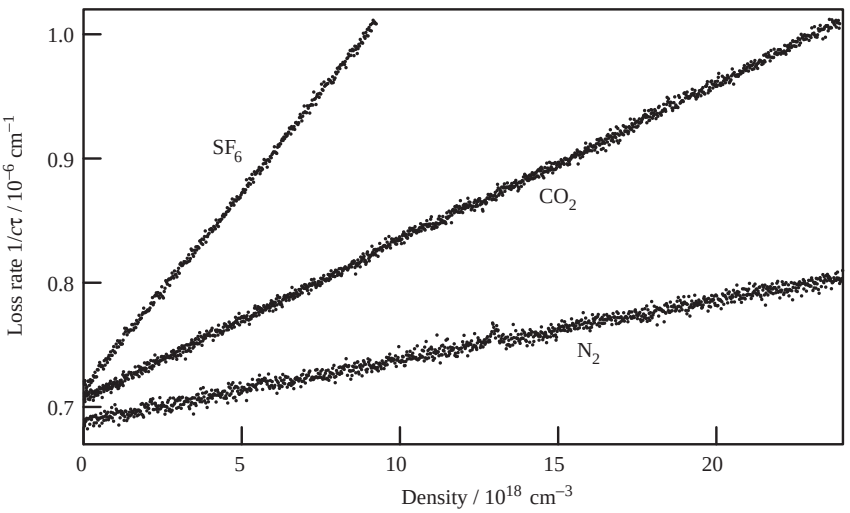

Fig. 1. Extinction as a function of the density in the cell for CO_2, SF_6 and N_2 at 18 788.4 cm^{-1}. The difference in offset for the empty cell is caused by a change in cleanliness of the mirrors, the water content of the dielectric layer and the particular alignment condition of the cavity.

unseeded Nd:YAG pump-laser was applied directly. Although several mirror sets were used, all mirrors had the same radius of curvature of 100 cm and reflectivities $\mathscr{R}_{\tilde{\nu}}$ exceeding 99.98%. The same cell was used to build all cavities, and the distance between the mirrors was 82 cm.

The flow of gas was controlled with a needle valve and the gas was purged through a sintered stainless steel filter with 0.5 μm pores to remove dust and aerosols. The cell has buffer chambers welded onto its side, to distribute the gas quickly and evenly throughout the cell. The cell and a mirror-mount is shown in Fig. 2. Smooth and slow pressurization of the cell is important to avoid turbulence. The needle valve was set in a way that a single pressurization scan of an evacuated cell up to 1 bar takes about 15 min. The pressure was measured by a capacitance manometer (Edwards 600 AB; 2 hPa accuracy) and recorded simultaneously with the decay rates. All measurements were performed at room temperature, at about 20 °C. A more accurate temperature of the cell is needed to calculate the density from the pressure. For this reason the temperature was measured as well, using a National Semiconductor LM50B sensor. The ideal gas law was used to calculate the density from the measured pressure and temperature. This introduces a negligible error of $<0.5\%$ at these densities.

A small but systematic underestimate of the scattering cross section is caused by forward and backward scattering. Light that is scattered back does not necessarily leave the cavity, but can continue to contribute to the ring down signal. The acceptance angle for this to occur is small, and the error is estimated to be less than 0.01%, taking into account the geometrical configuration (see also Fig. 3), the scattering distribution and the stability criterion of the cavity. In quantitative

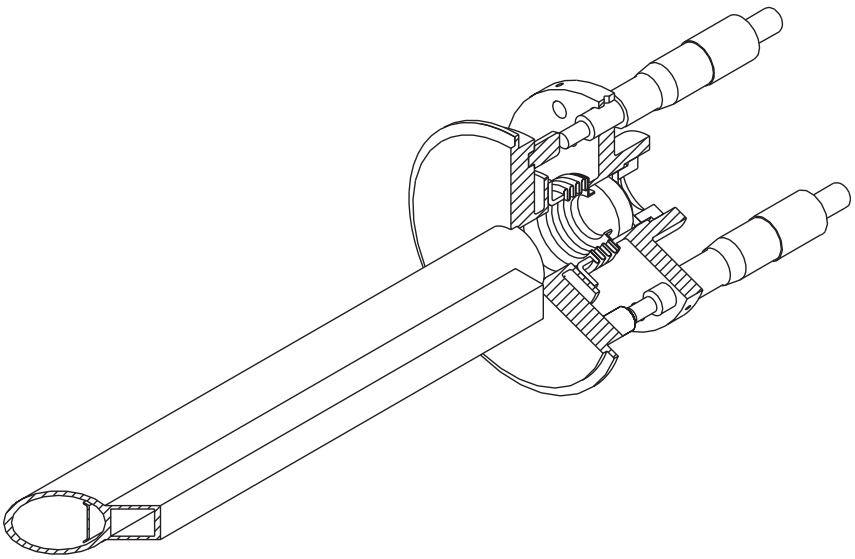

Fig. 2. Configuration of the absorption cell used in the experiment. The cell is sealed by mirrors (25.4 mm diameter) pressed against an O-ring, placed in an adjustable mount and aligned by micrometer screws to obtain a stable CRD resonator. A bellow allows for the necessary flexibility of the two plates with respect to each other and sealing between them. Gas is distributed from the rectangular chamber into the actual absorption chamber through a series of holes to obtain a homogeneous density distribution. To remove dust and aerosols the gas is purged in a stainless-steel filter with 0.5-μm pores.

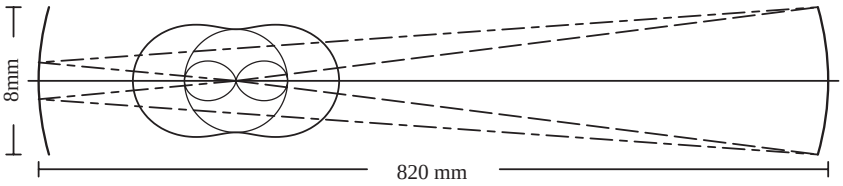

Fig. 3. A fraction of the scattered light will fulfill the stability criteria of the cavity and continue to circulate. Drawing not to scale.

CRD spectroscopy often the absorption cross section is underestimated in cases where the resonance linewidth is narrower than the excitation profile of the laser; this phenomenon is associated with non-exponential decays and it invalidates (Eq. 8). However, for the non-resonant phenomenon of Rayleigh scattering the linewidth problem of CRD spectroscopy is not an issue.

The Rayleigh scattering cross section follows from a linear fit of the loss rate $\beta_{\bar{\nu}}$ versus the density in the cell N following (Eq. 8). The slope of the plots shown in Fig. 1 directly yields a value for $\sigma_{\bar{\nu}}$. The reflectivity of the mirrors determine the vertical offset and the signal-to-noise ratio on the measurement. By means of these fitting procedures a large amount of data is used in subsequent fitting routines to extract a single value for a cross section.

4. Rayleigh scattering in argon, nitrogen and carbon dioxide between 17 500 and 21 400 cm^{-1}

The extinction due to Rayleigh scattering was measured over a wide frequency range in argon, nitrogen and carbon dioxide. In the analysis these measurements are combined with earlier results by Naus and Ubachs [14]. Thirteen new frequencies for argon, twenty three for nitrogen and twenty two for carbon dioxide ware added in the blue, as well as a further twenty five in the yellow region for carbon dioxide. The measurements performed with the second harmonic of the Nd:YAG pump laser are discussed in Section 5. The Rayleigh scattering cross sections, as determined from the decay rates are plotted in Figs. 4 and 5 as a function of frequency.

The measured Rayleigh scattering cross sections are compared to n-based cross sections. The refractive indices used in this procedure are scaled to the density at 15 °C and 1013 hPa, or $25.47 \times 10^{18}\,\mathrm{cm}^{-3}$. Also all presently obtained values are scaled to the same density for comparison. In the following sections we describe how values of refractive indices as well as depolarization ratios are obtained from literature.

4.1. Argon

Peck and Fisher [30] measured the refractive index in argon, resulting in a dispersion relation valid for the range $5000 < \bar{\nu} < 33\,000\,\mathrm{cm}^{-1}$.

$$(n-1)\times 10^8 = 6432.135 + \frac{286.06021 \times 10^{12}}{14.4 \times 10^9 - (\bar{\nu}/\mathrm{cm}^{-1})^2}. \tag{9}$$

Because argon is spherical, the King correction factor is taken to be unity.

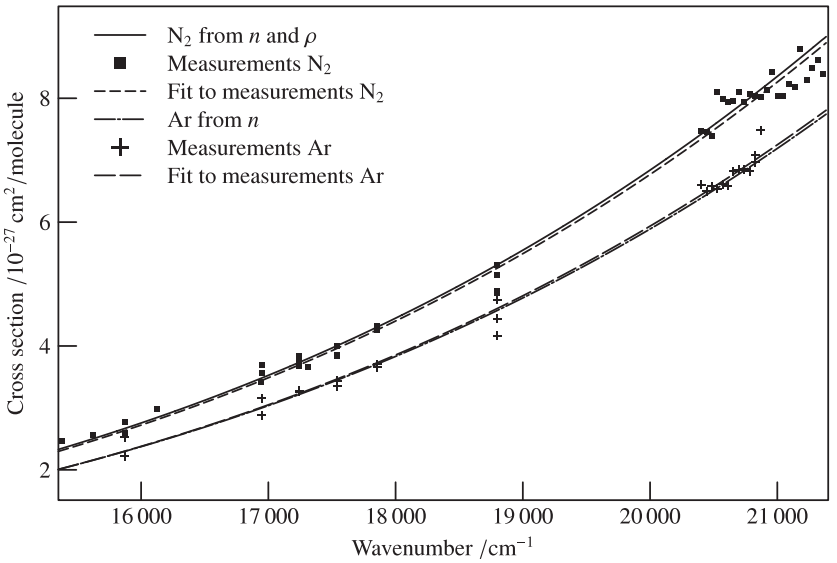

Fig. 4. Wavelength dependent Rayleigh scattering cross sections in Ar and N_2 between 15 400 and 21 400 cm^{-1}. The curves are calculated from the refractive index [30,8] and, in the case of N_2, the depolarization [8]. Fits of (Eq. 15) to the measured data are also shown.

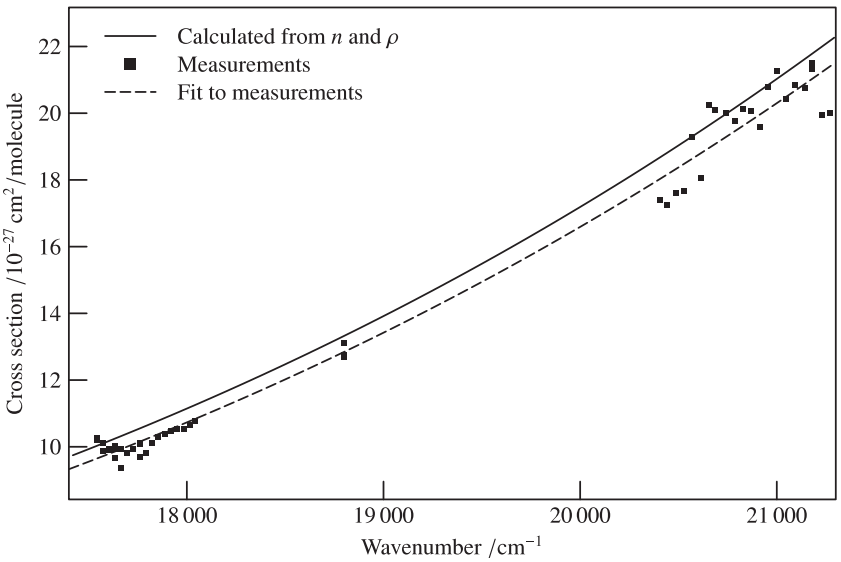

Fig. 5. Wavelength dependent Rayleigh scattering cross sections in CO_2 between 17 400 and 21 400 cm^{-1}. The drawn curve is calculated from a measured dispersion relation of the refractive index [33] and the King correction factor, (Eq. 14). Fits of (Eq. 15) to the measured data are also shown.

4.2. Nitrogen

The value of the refractive index of nitrogen in the wavelength range $468 \leqslant \lambda_{\mathrm{vac}} \leqslant 2059\,\mathrm{nm}$ was measured by Peck and Khanna [31] yielding a dispersion relation:

$$(n-1)\times 10^8 = 6498.2 + \frac{307.43305\times 10^{12}}{14.4\times 10^9 - (\bar{\nu}/\mathrm{cm}^{-1})^2}, \quad 4860\,\mathrm{cm}^{-1} < \bar{\nu} < 21\,360\,\mathrm{cm}^{-1} \tag{10}$$

after scaling to 15 °C and 1013 hPa. Bates [8] gives a dispersion relation for slightly shorter wavelengths, as an interpolation between values of Ref. [31] and measurements by Abjean et al. [32] in the ultraviolet.

$$(n-1)\times 10^8 = 5677.465 + \frac{318.81874\times 10^{12}}{14.4\times 10^9 - (\bar{\nu}/\mathrm{cm}^{-1})^2}, \quad 21\,360\,\mathrm{cm}^{-1} < \bar{\nu} < 39\,370\,\mathrm{cm}^{-1}. \tag{11}$$

Nitrogen is a non-spherical molecule and has therefore a non-zero depolarization. Bates [8] gives a dispersion relation for the King correction factor $F_{\mathrm{k}}(\bar{\nu})$, based on measurements by Alms et al. [16] and Bridge and Buckingham [21] and calculations by Oddershede and Svendsen [26] yielding:

$$F_{\mathrm{k}}(\bar{\nu}) = 1.034 + 3.17\times 10^{-12}(\bar{\nu}/\mathrm{cm}^{-1})^2. \tag{12}$$

4.3. Carbon dioxide

Bideau-Mehu et al. [33] have measured the refractive index of CO_2 using an interferometric technique. Their article contains a typographical error, and the corrected formula, scaled to 15 °C and 1013 hPa, yields:

$$(n-1) = 1.142\,7\times 10^6\left(\frac{5\,799.25}{(128\,908.9)^2 - (\bar{\nu}/\mathrm{cm}^{-1})^2} + \frac{120.05}{(89\,223.8)^2 - (\bar{\nu}/\mathrm{cm}^{-1})^2} + \frac{5.333\,4}{(75\,037.5)^2 - (\bar{\nu}/\mathrm{cm}^{-1})^2} + \frac{4.324\,4}{(67\,837.7)^2 - (\bar{\nu}/\mathrm{cm}^{-1})^2} + \frac{0.121\,814\,5\times 10^{-4}}{(2418.136)^2 - (\bar{\nu}/\mathrm{cm}^{-1})^2}\right). \tag{13}$$

Because of the linear configuration of the CO_2 molecule, a large depolarization is expected. Alms et al. [16] have performed measurements of the depolarization, and with the aid of (Eq. 7) the King correction factors were calculated. The parameters of the model function used by Bates [8] for N_2 was then fitted to obtain a dispersion relation for the King correction factor in CO_2.

$$F_{\mathrm{k}}(\bar{\nu}) = (1.1364 \pm 0.0005) + (25.3 \pm 1.5)\times 10^{-12}\,(\bar{\nu}/\mathrm{cm}^{-1})^2. \tag{14}$$

The differences between (Eq. 14) and the measured King correction factors are less than 0.5%. Since the measurements by Alms et al. [16] cover a wider frequency range than our spectrum, no extrapolation was needed, and the same accuracy is assumed for the entire frequency range. A plot representing the fit to interpolate a value for the depolarization is shown in Fig. 7.

4.4. Analysis

The larger frequency range in the present work with respect to the range covered by Naus and Ubachs [14] allows for better verification of the frequency dependence of the scattering cross section. The Rayleigh scattering cross section is not exactly proportional to $\bar{\nu}^4$, due to both the dispersion of the refractive index and the King correction factor. Several authors have suggested a variety of fitting equations to account for this difference. From Teillet [34] the following equation to describe frequency dependence of the Rayleigh scattering is taken:

$$\sigma_{\bar{\nu}} = \bar{\sigma}\,(\bar{\nu}/\mathrm{cm}^{-1})^{(4+\delta)}, \tag{15}$$

where δ accounts for the dispersion in both the refractive index and the King correction factor. The disadvantage of (Eq. 15) is that the contributing factors are not clearly separated, but it can be fitted to the measured cross sections and allows for comparison to the cross sections that are calculated from the refractive indices and depolarization ratios. The theoretical values were found using a fit on a large number of points computed using (Eq. 2) in the range 10 000 to 25 000 cm^{-1}. An unfortunate property of (Eq. 15) is that the correlation between the two parameters is very strong, leading to unacceptable error margins on the fitted parameters. To find the experimental values in Table 1, one parameter was held fixed to the theoretical value, while the other was optimised to yield the least-squares difference. After two iterations of fitting one variable and holding the other and then interchanging the free and fixed variables, the values no longer changed.

The last column in Table 1 is the relative mean difference between the measured cross sections and those derived from the refractive index:

$$\Delta_{\mathrm{avg}} = \frac{1}{n}\sum_{i=1}^{n}\frac{\sigma^{\mathrm{exp}}(\bar{\nu}_i) - \sigma^{n\text{-based}}(\bar{\nu}_i)}{\sigma^{\mathrm{exp}}(\bar{\nu}_i)} \tag{16}$$

with $\sigma^{\mathrm{exp}}(\nu_i)$ our experimental Rayleigh scattering cross section at wavenumber $\bar{\nu}_i$ and $\sigma^{\mathrm{refr}}(\bar{\nu}_i)$ the Rayleigh scattering cross section calculated from Eqs. (2) and (7) with the appropriate reference data at the same position. Hence the agreement between the measured scattering cross sections in Ar and N_2 and the n-based scattering cross sections is better than 1%. The agreement for carbon dioxide is less good, at about 4%. A possible source for the deviation is the lack of knowledge about the large King correction factor in the order of 1.15, which may be prone to some error.

Table 1
Values for the parameters in (Eq. 15)

Gas	$\bar{\sigma}_{n\text{-based}}$ $/10^{-47}$	$\bar{\sigma}_{\mathrm{exp}}$ $/10^{-47}$	$\delta_{n\text{-based}}$	δ_{exp}	$\Delta_{\mathrm{avg}}(\%)$
Ar	14.68(3)	14.21(8)	0.0930(2)	0.0968(5)	0.4
N_2	16.31(4)	18.83(9)	0.974(3)	0.0817(5)	−0.7
CO_2	28.49(9)	27.42(14)	0.1343(3)	0.1343(5)	−3.9

Values in parentheses are 1 σ errors in the last digits.

5. Rayleigh scattering in CO_2, N_2, Ar, N_2O, CH_4, CO, SF_6 at 532 nm

The output of the second harmonic of an unseeded Nd:YAG laser, with a bandwidth of $1\,cm^{-1}$, was used to measure scattering cross sections at a fixed frequency of $18\,788.4 \pm 0.4\,cm^{-1}$, corresponding to 532.2 nm. Three typical pressure ramps are already shown in Fig. 1. The results on the Rayleigh scattering cross sections, derived from the slopes in the pressure ramp curves and averaged over several traces, are listed in Table 2. For CO_2, N_2, Ar, N_2O, CH_4, CO and SF_6. Again a comparison will be made with *n*-based cross sections. The dispersion relations for the King correction factor and the refractive index for argon, nitrogen and carbon dioxide have been discussed in the above. For the other gases equations for the refractive index and the depolarization were found in literature, or fitted to data taken from literature. Each of the gases will be discussed below. Figs. 6 and 7 show graphical representations of the fits used to obtain the dispersion relations for refractive indices and depolarization factors. The refractive index depends on the density, and the values given here are again scaled to 15 °C and 1013 hPa, or a density of $25.47 \times 10^{18}\,cm^{-3}$.

5.1. Carbon monoxide

The value of the refractive index of carbon monoxide in the wavelength range $168 \leqslant \lambda_{vac} \leqslant 288$ nm was measured by Smith et al. [27]. A functional form similar to the dispersion relation for nitrogen and argon was fitted to these 38 data points (see also Fig. 6):

$$(n-1) \times 10^8 = (22\,851 \pm 200) + \frac{(0.456 \pm 0.01) \times 10^{12}}{(71\,427 \pm 200)^2 - (\bar{\nu}/cm^{-1})^2}. \quad (17)$$

Note that the extrapolation to 532 nm is rather far outside the range of the measurements, and that the authors did not fit a dispersion relation to their data. Within the range of the measurements, the accuracy of $n-1$ is estimated to be $\sim 2\%$.

Table 2
Scattering cross sections at $18\,788.4\,cm^{-1}$

Gas	Measured $\sigma_{\bar{\nu}}$ $/10^{-27}\,cm^2$	*n*-based $\sigma_{\bar{\nu}}$ $10^{-27}\,cm^2$	$(n-1)^a$ $/10^{-6}$	$F_k(\bar{\nu})^b$	Purity of the gas (%)	#[c]
Ar	4.45 (0.3)	4.56	268	1	99.999	3
N_2	5.10 (0.24)	5.30	284	1.035	99.9	3
CO	6.19 (0.4)	6.82	325	1.016	99.997	3
CO_2	12.4 (0.8)	13.29	427	1.145	99.7	4
CH_4	12.47 (0.23)	14.69	481	1.000	99.5	3
N_2O	15.90 (0.08)	18.19	483	1.225	99.7	2
SF_6	32.3 (0.5)	34.1	733	1.000	99.8	2

Figures in parentheses give the $1\,\sigma$ uncertainty.
[a] At 15 °C and 101 325 Pa. References are given in the text.
[b] References are given in the text.
[c] Number of pressure ramps.

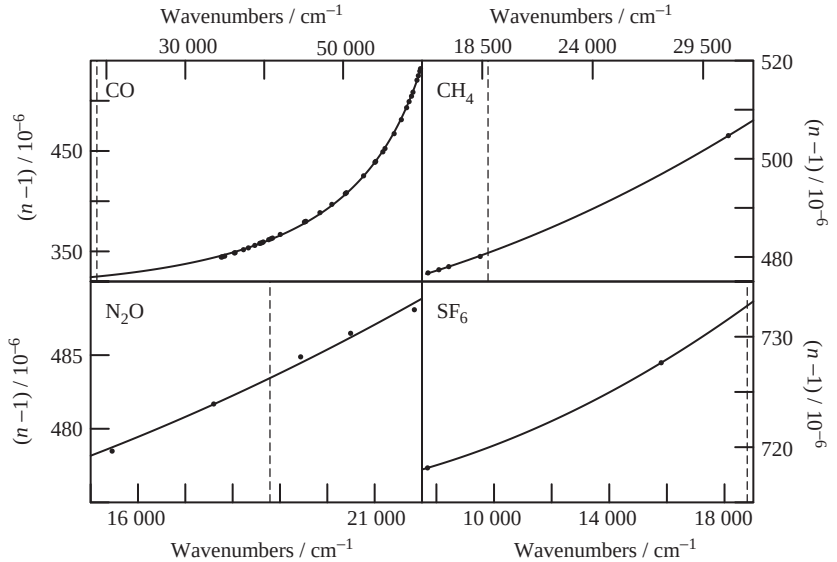

Fig. 6. Fits of the refractive index against measured data. The dashed vertical lines indicate the frequency of the second harmonic of a Nd:YAG laser. Details are given in the text. Refs: CO from [27]; CH_4 from [35]; N_2O from [16]; SF_6 from [36].

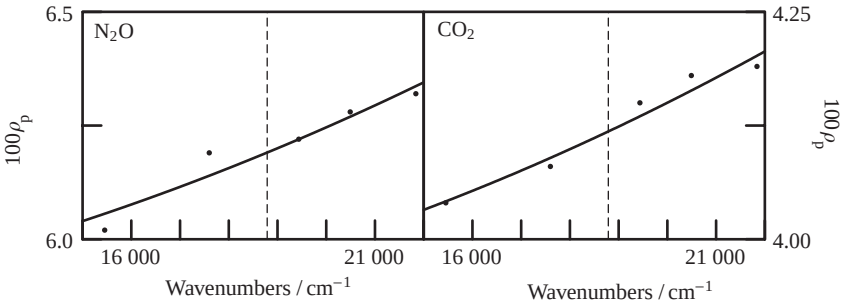

Fig. 7. The fits of the depolarization ratio ρ_n against measured data. The dashed vertical lines indicate the frequency of the second harmonic of an Nd:YAG laser. All measurements were taken from Alms et al. [16]. Details are given in the text.

Because carbon monoxide is a diatomic molecule, its depolarization is not zero. A single measurement of the depolarization ratio was found at $\lambda = 632.8$ nm yielding $\rho_p = 0.0048$ [21]. Ab initio calculations have shown that the dispersion in the depolarization ratio can be neglected [26], and therefore the value at the He–Ne laser wavelength was used for the calculations in Table 2.

5.2. Methane

Measurements of the polarizability by Hohm [35] were used to fit a dispersion relation for the refractive index. Since the number of data points was much smaller than in the case of carbon

monoxide, a simpler function was chosen:

$$(n-1)\times 10^8 = (46\,662 \pm 13) + (4.02 \pm 0.03)\times 10^{-6}\,(\bar{\nu}/\mathrm{cm}^{-1})^2. \tag{18}$$

The accuracy of this equation is estimated to be better than 4% in the range of the source data. For our 532 nm measurements, an interpolation is needed, with the same 4% accuracy assumed.

Measurements of the polarizability anisotropy were not found, but Bridge and Buckingham [21] performed measurements on CCl_4 and found a depolarization ρ_p of less than 0.2×10^{-3}, leading to a King correction factor with a negligible difference from unity. The same symmetry is present in CH_4 and in CCl_4 and therefore it is assumed that methane has the same depolarization.

5.3. Nitrous oxide

This gas was chosen because of its known high depolarization ratio. Measurements of the polarizability by Alms et al. [16], yielded both the refractive index and the depolarization ratio:

$$\rho_p = (0.0577 \pm 0.0007) + (11.8 \pm 2)\times 10^{-12}\,(\bar{\nu}/\mathrm{cm}^{-1})^2, \tag{19}$$

$$(n-1)\times 10^8 = (46\,890 \pm 85) + (4.12 \pm 0.2)\times 10^{-6}\,(\bar{\nu}/\mathrm{cm}^{-1})^2. \tag{20}$$

5.4. Sulphur hexafluoride

This is the gas with the largest known polarizability. Unfortunately, exactly how large it is only known at two optical frequencies and in the static limit. The two optical frequencies—633 and 1300 nm—from Vukovic et al. [36] were used to extract the two constants for the dispersion relation:

$$(n-1)\times 10^8 = 71\,517 + 4.996\times 10^{-6}\,(\bar{\nu}/\mathrm{cm}^{-1})^2. \tag{21}$$

Because of the lack of measurements an extrapolation to short wavelength only provides a crude approximation, for comparison only. Bridge and Buckingham [21] performed measurements on the depolarization in SF_6 and found a value for ρ_p of less than 0.2×10^{-3}, leading to a King correction factor with a negligible difference from unity.

5.5. Analysis

The comparison between measured and n-based cross sections in Table 2 shows that the present values are lower by a few % for Ar, N_2 and CO_2, while deviations are larger for the other gases, up to 15% for CH_4. We do not have an explanation for the obtained differences. Nevertheless the present measurements provide an independent verification of Rayleigh scattering cross sections, at least to the several % accuracy level.

6. Extinction in O_2 at 532 nm

Measurements on oxygen at 532.2 nm using the CRD setup and the pressure ramp method yield a nonlinear behavior of the cavity loss-rate with respect to density as shown in Fig. 8. This phenomenon is not unexpected, since collision-induced absorption features in O_2 are well documented [37,38]. Also in our group CRD-spectroscopy was applied to record the collision-induced profiles and cross sections of O_2–O_2 at 570 and 630 nm [39] and at 477 nm [40]. The feature at 532 nm is known to correspond to the $a^1\Delta_g(v'=0)+a^1\Delta_g(v'=2) \leftarrow X^3\Sigma_g^- + X^3\Sigma_g^-$ transition. In fact both Greenblatt et al. [37] and Newnham and Ballard [38] report the wavelength of 532.2 nm to exactly coincide with the peak of this collisional absorption feature.

For measurements involving collision-induced absorptions, the density dependent losses in the cavity can be expressed as:

$$\beta_{\bar{\nu}}(N) = \beta_{\bar{\nu}}^0 + c\,\sigma_{\bar{\nu}}^{\mathrm{R}} N + c\,\sigma^{\mathrm{CIA}}\,N^2, \tag{22}$$

where $\beta_{\bar{\nu}}^0$ represent mirror losses, the second term with $\sigma_{\bar{\nu}}^{\mathrm{R}}$ relates to Rayleigh scattering, and the third term involves the collisional absorption cross section σ^{CIA} scaling with N^2. In Fig. 8 this quadratic dependence on the density is clearly visible. The drawn line in the same graph is the prediction of a pressure ramp if the quadratic collision-induced absorption were not present. The Rayleigh scattering cross section can either be extracted from the measurements like the one presented in Fig. 8 or an n-based value can be invoked. A three-component fit results in a value $\sigma_n^{\mathrm{R}} = (4.50 \pm 0.15) \times 10^{-27}\,\mathrm{cm}^2$. Alternatively a value for σ_n^{R} can be derived from the dispersion relations, which can subsequently be used in a two-component fir.

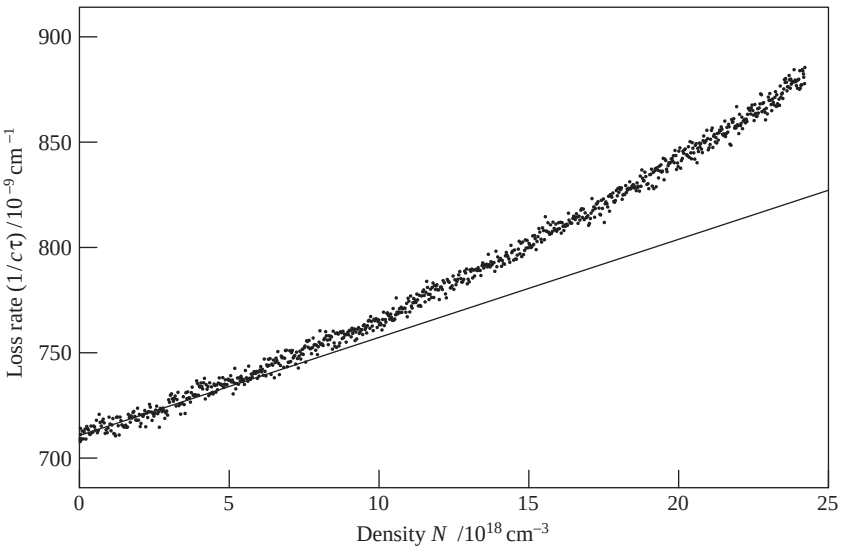

Fig. 8. Pressure ramp in oxygen. The non-linear behavior is clearly visible. For comparison, the calculated pressure ramp for oxygen is drawn as well—the straight line, with the slope calculated from refractive index and King correction factor taken from Bates [8].

Bates [8] combines the measurements of several groups into a dispersion relation for oxygen, yielding for vacuum wavelengths $546 > \lambda_{vac} > 288$ nm:

$$(n-1)\times 10^8 = 20\,564.8 + \frac{24.808\,99}{4.09\times 10^9 - (\bar{\nu}/\mathrm{cm}^{-1})^2}. \tag{23}$$

From Bates [8], we reproduce an expression for the wavelength-dependent King correction factor, based again on a combination of sources, both measurements and ab initio calculations.

$$F_k(\bar{\nu}) = 1.096 + 1.385\times 10^{-11}(\bar{\nu}/\mathrm{cm}^{-1})^2 + 1.448\times 10^{-20}(\bar{\nu}/\mathrm{cm}^{-1})^2. \tag{24}$$

Based on these expressions and parameters a scattering cross section of $4066\times 10^{-27}\,\mathrm{cm}^2$ results at 532.2 nm. With this value fixed for the linear contribution the quadratic contribution, associated with collisional absorption can be derived from a two-component fit. This procedure results in a value for the collision-induced absorption cross section $\sigma^{CIA} = (1.01\pm 0.03)\times 10^{-46}\,\mathrm{cm}^5\,\mathrm{molecule}^{-2}$. Greenblatt et al. [37] and Newnham and Ballard [38] have performed measurements of the same absorption feature and they found a peak-height of $(1.0\pm 0.03)\times 10^{-46}$ and $(1.23\pm 0.38)\times 10^{-46}\,\mathrm{cm}^5\,\mathrm{molecule}^{-2}$, respectively. The position of the transition indicated in both articles is 532.2 nm or $18\,790\,\mathrm{cm}^{-1}$, within the error margins coincident with the frequency of the Nd:YAG laser presently used. Also in previous studies by our group on three other O_2–O_2 collisional-induced features [39,40] a better agreement was found with the results of Greenblatt et al. [37] than with the results of Ref. [38].

7. Conclusions

We have measured the Rayleigh scattering cross section in Ar, N_2 and CO_2 by a direct method over an extended wavelength range. We find an agreement with values calculated from the refractive index and the King correction factor to within 1%, except for CO_2, where the error is about 4%. The measurements of the Rayleigh scattering cross sections in CO_2, N_2, Ar, N_2O, CH_4, CO and SF_6 at the wavelength of the second harmonic of an Nd:YAG laser can be useful for LIDAR experiments. These measurements show larger differences between values calculated from the refractive index and the depolarization ratio. This is in part because the measured refractive indices and depolarization ratios are incomplete. In O_2 the second harmonic of the Nd:YAG laser coincides with a collision-induced resonance, and the measured strength of this transition agrees with values found in literature.

Acknowledgements

The authors wish to thank the Space Research Organisation Netherlands (SRON) for a Grant (EO-036) in the Earth Observation program.

References

[1] Strutt JW(Lord Rayleigh). On the transmission of light through an atmosphere containing small particles in suspension, and on the origin of the blue of the sky. Philos Mag 1899;47:375–84
Reprinted in: Lord Rayleigh, Scientific papers, Part IV, New York: Dover Publications; 1964. p. 397.

[2] van de Hulst HC. Light scattering by small particles. New York: Dover Publications; 1981.
[3] Fabilinskii IL. Molecular scattering of light. New York: Plenum; 1968.
[4] Penney CM. Light scattering in terms of oscillator strengths and refractive indices. J Opt Soc Am 1969;59:34–42.
[5] Young AT. Rayleigh scattering. Appl Opt 1981;20:533–5.
[6] Chandrasekar S. Radiative transfer. New York: Dover Publications; 1950.
[7] Miles RB, Lempert WR, Forkey JN. Laser Rayleigh scattering. Meas Sci Technol 2001;12:R33–51.
[8] Bates RD. Rayleigh scattering by air. Planet Space Sci 1984;32:785–90.
[9] Bucholtz A. Rayleigh-scattering calculations for the terrestrial atmosphere. Appl Opt 1995;34:2765–73.
[10] Jackson JD. Classical electrodynamics, 3rd ed. New York: Wiley; 1999.
[11] Strutt RJ. The light scattered by gases: its polarisation and intensity. Proc Roy Soc London 1918;95:155–76.
[12] Strutt RJ. A re-examination of the light scattered by gases in respect of polarisation. I. Experiments on the common gases. Proc Roy Soc London 1920;97:435–50.
[13] King LV. On the complex anisotropic molecule in relation to the dispersion and scattering of light. Proc Roy Soc London 1923;104:333–57.
[14] Naus H, Ubachs W. Experimental verification of Rayleigh scattering cross sections. Opt Lett 2000;25:347–9.
[15] Hohm U, Kerl K. Interferometric measurements of the dipole polarizability α of molecules between 300 K and 1100 K I. Monochromatic measurements at $\lambda = 632.99$ nm for the noble gases and H_2, N_2, O_2 and CH_4. Mol Phys 1990;69:803–17.
[16] Alms GR, Burnham AK, Flygare WH. Measurement of the dispersion in polarizability anisotropies. J Chem Phys 1975;63:3321–6.
[17] Boyd RW. Nonlinear optics. San Diego: Academic Press; 1992.
[18] Herzberg G. Molecular spectra and molecular structure I. Diatomic molecules, 2nd ed. London: Van Nostrand Reinhold; 1950.
[19] Moosmüller H. Optical absorption in nitrogen due to spontaneous Raman scattering. J Opt Soc Amer B 1994;11:286–9.
[20] Knippers W, van Helvoort K, Stolte S. Vibrational overtones of the homonuclear diatoms (N_2, O_2, D_2) observed by the spontaneous Raman effect. Chem Phys Lett 1985;121:279–86.
[21] Bridge NJ, Buckingham AD. The polarization of laser light scattered by gases. Proc R Soc A 1966;295:334–49.
[22] Penney CM, St. Peters RL, Lapp M. Absolute rotational Raman cross sections for N_2, O_2 and CO_2. J Opt Soc Am 1974;64:712–5.
[23] Ford AL, Browne JC. Direct-resolvent-operator computations on the hydrogen-molecule dynamic polarizability, Rayleigh, and Raman scattering. Phys Rev A 1973;7:418–26.
[24] Rychlewski J. An accurate calculation of the polarizability of the hydrogen molecule and its dependence on rotation, vibration and isotopic substitution. Mol Phys 1980;41:833–42.
[25] Langhoff SR, Bauschlicher Jr. CW. Theoretical study of the effects of vibrational-rotational interactions on the Raman spectrum of N_2. J Chem Phys 1983;78:5287–92.
[26] Oddershede J, Svendsen EN. Dynamic polarizabilities and Raman intensities of CO, N_2, HCl and CL_2. Chem Phys 1982;64:359–69.
[27] Smith PL, Huber MCE, Parkinson WH. Refractivities of H_2, He, O_2, CO and Kr for $168 \leqslant \lambda \leqslant 288$ nm. Phys Rev A 1976;13:1422–34.
[28] Berden G, Peeters R, Meijer G. Cavity ring-down spectroscopy: experimental schemes and applications. Int Rev Phys Chem 2000;19:565–607.
[29] Naus H, van Stokkum IHM, Hogervorst W, Ubachs W. Quantitative analysis of decay transients applied to a multimode pulsed cavity ringdown experiment. Appl Opt 2001;40:4416–26.
[30] Peck ER, Fisher DJ. Dispersion of Argon. J Opt Soc Am 1964;54:1362–4.
[31] Peck ER, Khanna BN. Dispersion of Nitrogen. J Opt Soc Am 1966;56:1059–63.
[32] Abjean R, Mhu A, Johannin-Gilles A. Mesure interfromtrique des indices de rfraction de l'azote et de l'argon dans l'ultraviolet. C R Acad Sci Paris 1970;271:411–4.
[33] Bideau-Mehu A, Guern Y, Abjean R, Johannin-Gilles A. Interferometric determination of the refractive index of carbon dioxide in the ultraviolet region. Opt Commun 1973;9:432–4.
[34] Teillet PM. Rayleigh optical depth comparisons from various sources. Appl Opt 1990;29:1897–900.

[35] Hohm U. Experimental determination of the dispersion in the mean linear dipole polarizability $\alpha(\omega)$ of small hydrocarbons and evaluation of Cauchy moments between 325 nm and 633 nm. Mol Phys 1993;78:929–41.
[36] Vukovic D, Woolsey GA, Scelsi GB. Refractivities of SF_6 and SOF_2 at wavelengths of 632.99 and 1300 nm. J Phys D 1996;29:634–7.
[37] Greenblatt GD, Orlando JJ, Burkholder JB, Ravishankara AR. Absorption measurements of oxygen between 330 and 1140 nm. J Geophys Res 1990;95:18577–82.
[38] Newnham DA, Ballard J. Visible absorption cross sections and integrated absorption intensities of molecular oxygen (O_2 and O_4). J Geophys Res 1998;103:28801–15.
[39] Naus H, Ubachs W. Visible absorption bands of the $(O_2)_2$collision complex at pressures below 760 Torr. Appl Opt 1999;38:3423–8.
[40] Sneep M, Ubachs W. Cavity Ring-Down Measurements of the O_2–O_2 collision induced absorption resonance at 477 nm at sub-atmospheric pressures. J Quant Spectrosc Radiat Transfer 2003;78:171–8.